International Journal of Nanomedicine

Dovepress
open access to scientific and medical research

Open Access Full Text Article

ORIGINAL RESEARCH

A Novel and Rapid Smear Cytomorphology Detection Strategy Based on Upconversion Nanoparticles Immunolabeling Integrated with Wright's Staining for Accurate Diagnosis of Leukemia

Lu Chen[1,*], Yu Zhong[2,*], Yong-Sheng Li[3], He Zhuang[4], Xin Li[5], Sheng-Ping Liu[5], Jing-Gang Li[5], Qiu Lin[4], Fei Gao[5]

[1]Department of Paediatrics, Fujian Maternity and Child Health Hospital, College of Clinical Medicine for Obstetrics and Gynecology and Pediatrics, Fujian Medical University, Fuzhou, 350000, People's Republic of China; [2]Department of Pharmaceutical Analysis, Faculty of Pharmacy, Fujian Medical University, Fuzhou, 350122, People's Republic of China; [3]Department of Urology, Fujian Medical University Union Hospital, Fuzhou, 350001, People's Republic of China; [4]Department of Clinical Laboratory, Fujian Medical University Union Hospital, Fuzhou, 350001, People's Republic of China; [5]Fujian Institute of Hematology, Fujian Provincial Key Laboratory on Hematology, Fujian Medical University Union Hospital, Fuzhou, 350001, People's Republic of China

*These authors contributed equally to this work

Correspondence: Fei Gao, Email xuzhougaofei@126.com

Background: Accurate, sensitive, and rapid identification of leukemia cells in blood and bone marrow is of paramount significance for clinical diagnosis. An integrative technique combining traditional cytomorphology with immunophenotyping was proposed to improve the diagnostic efficiency in leukemia. On account of high photostability, biocompatibility, and signal-to-background ratio, upconversion nanoparticles (UCNPs) as luminescent labels have drawn substantial research scrutiny in immunolabeling.

Methods: To achieve simultaneous determination, $NaYF_4$:Yb,Er UCNPs were coupled with CD38 antibodies to construct immunofluorescence probes that were developed to bind to diffuse large B cell lymphoma (DLBCL) cells, followed by Wright's staining that has been widely used in clinical work for morphological diagnosis. Further, the experimental conditions were optimized, such as medium, slice-making method, antibody dosage, incubation time, etc.

Results: The cell morphology and immunolabeling could be observed simultaneously, and its simple operation rendered it a possibility for clinical diagnosis. The developed immunolabeling assay could achieve DLBCL cell counting with high reproducibility and stability, and the detection limit was as low as 1.54 cell/slice (>3 σ/s). Moreover, the proposed method also realized real blood and bone marrow sample analysis, and the results were consistent with the clinical diagnosis.

Conclusion: Overall, this strategy can be carried out after simple laboratory training and has prospective biomedical applications in leukemia classification, diagnosis validation, and differential diagnostics.

Keywords: leukemia, upconversion nanoparticle, immunofluorescence probe, Wright's staining, cytomorphology

Introduction

Leukemia, a generic term, encompasses several life threatening malignant disorders that present with incremental amounts of leucocytes in blood and bone marrow. Leukemia cells have the innate ability for migration and invasion.[1] Dedifferentiated and malignant leucocytes not only retain the benign leucocytes capacity for cell motility and survival in the circulation, but obtain the potential for rapid and uncontrolled cell division.[1] Accordingly, leukemia is aggressive and is a challenging disease to treat. Regrettably, leukemia may occur at all ages from the newborn to the aged with different forms and various age distributions.[2] Rapid and accurate diagnosis of leukemia is vital to prevent disease progression and reduce mortality.

Currently, the common diagnostic techniques toward leukemia principally lean on cytomorphology, cytochemistry, immunophenotyping (flow cytometry, FCM), cytogenetics (chromosome analysis and fluorescence in situ hybridization),

Received: 18 April 2023
Accepted: 3 September 2023
Published: 13 September 2023

Graphical Abstract

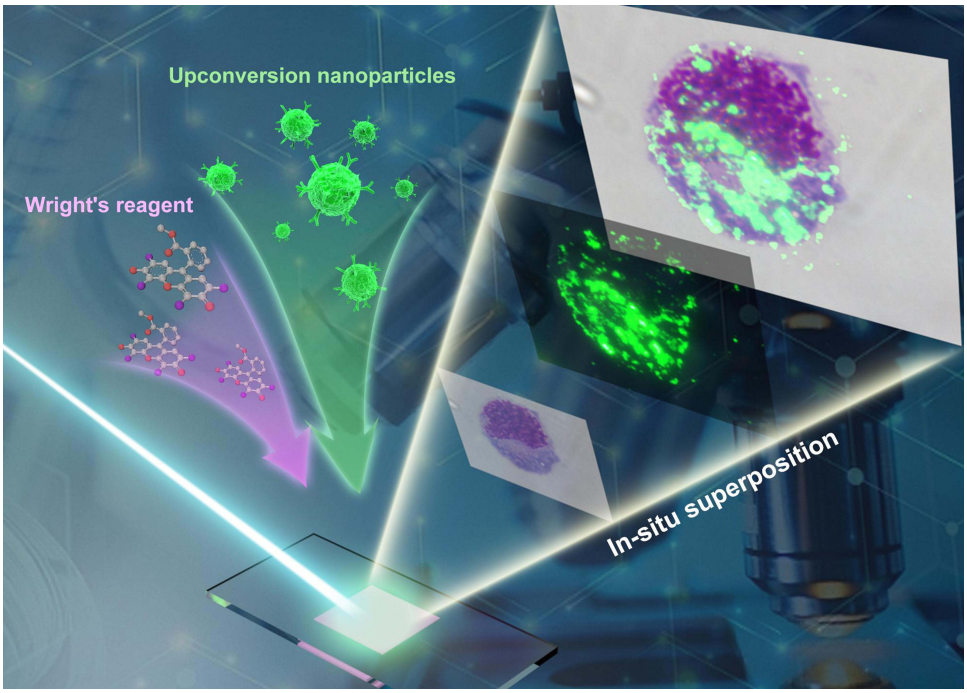

and molecular genetics (polymerase chain reaction and sequencing technique).[3–5] Regrettably, there is a shortage of FCM equipment, and other cytogenetics and molecular genetics methods available at laboratory diagnostic centers require expensive equipment, experienced personnel, immediate processing, tedious operation, and so on.[6,7] Correspondingly, cytomorphology is an indispensable approach in hematological disease diagnosis owing to its fast evaluation of specimens, thus endowing time-saving and cost-effective characteristics. Specifically, trained hematologists can distinguish abnormalities in cell morphology or potential leukemia cells from normal counterparts.[8] Further, assessment of the percentage and relative distribution of erythropoiesis, granulopoiesis, and monocytopoiesis can identify a series of hematological diseases.[9] Accompanied by cytochemical staining, cell lineage determination and dysplasia evaluation have been facilitated in many cases. Taken together, cytomorphology is vital for classification and diagnosis of leukemia.

However, there is a significant discordance in the morphological diagnosis of leukemia given by different laboratories, even within the same laboratory, due to the subjective nature of morphological classification and lack of standardization. Generally, considering the comprehensive and complementary characterization of each case, multidisciplinary diagnosis is imperative. Leukemia immunophenotyping also plays an important role in cell lineage identity and evaluation of the degree of maturation.[9,10] In this regard, immunophenotyping integrated with cytomorphology can enhance the diagnostic coincidence rate, reduce costs, and streamline the process, which is envisioned to be applied in cooperative diagnosis of leukemia. The frequently-used immunophenotyping technique is FCM, that uses cluster of differentiation (CD)-lineage specific antibodies to identify the lineage of leukemia, but it still has some weaknesses, such as time consumption, high cost, and complex operation.[11] Importantly, the immunofluorescence labeling technique, with merits of rapidness, high specificity, sensitivity, and simple operation, is a credible alternative. Luminescent materials are essential to achieve high resolution, signal-to-noise, and sensitivity. Traditional luminescent materials (such as organic fluorescent dyes, fluoresceins, and semiconductor quantum dots) exist with some intrinsic limitations, such as strong autofluorescence, rapid photobleaching, low chemical stability, severe toxicity, and so forth.[12–15] Accordingly, these materials are hard to meet the requirements of immunolabeling and identification of leukemia cells, and novel luminescent materials are urgently needed. Lanthanide ions-doped upconversion nanoparticles (UCNPs) emerged as

a promising fluorescent probe, converting a longer wavelength radiation (near-infrared and infrared light) into a shorter wavelength fluorescence (visible light) that can effectively avoid the interference of autofluorescence and scattering light of biological samples to improve the sensitivity.[16,17] Moreover, UCNPs exhibit high chemical stability, excellent biocompatibility, long lifetime emission, minimum photo-damage, and so on, which are widely employed in immunoassays and bioimaging.[18–20] For instance, Gorris et al[21] presented a protocol for synthesis of UCNPs in various sizes to yield tunable light emission that can eliminate optical background interference, and for the conjugation of streptavidin or antibodies for blood-based biomarkers determination. Minh et al[22] constructed $NaYF_4$:Yb,Er nanoparticles coated with silica and D-α-tocopheryl polyethylene glycol 1000 succinate for highly specific binding to breast cancer cells rather than healthy cells.

In this work, a novel and rapid smear detection strategy based on cytomorphology and immunophenotyping was developed for leukemia cells detection. As a proof-of-concept, CD38 was chosen due to its high expression in diffuse large B cell lymphoma (DLBCL).[23] Specifically, as shown in Figure 1, we adopted $NaYF_4$:Yb,Er UCNPs coupled with CD38 antibodies to construct UCNPs-CD38 immunoflurescence probes for DLBCL cells labeling, accompanied by cytochemical Wright's staining. The medium, slice-making method, antibody dosage, and incubation time were optimized. Through processing with Image J software, the analytical performance of this method was investigated. The synergetic recognition method of cell morphology and immunolabeling was successfully employed in patients' blood and bone marrow sample analysis. Taken together, the proposed synchronous detection tactic is expected to be used for accurate, economical, and rapid determination of cell properties and diagnosis of leukemia.

Experimental Sections

Reagents and Apparatus

Erbium acetate hydrate, ytterbium acetate, 1-octadecene (ODE, 90%), bovine serum albumin (BSA), N-ethyl-N'-(3-(dimethylamino)propyl) carbodiimide (EDC), N-hydroxysuccinimide (NHS), 2-morpholinoethanesulfonic acid (MES) and polyacrylic acid (PAA) were purchased from Sigma-Aldrich (St Louis, USA). Yttrium acetate tetrahydrate and oleic acid (OA) were obtained from Alfa Aesar (Shanghai, China). Sodium acetate (AR) and sodium bifluoride were obtained from Aladdin Reagent Co., Ltd (Shanghai, China). Ethanol, methanol, acetone, and cyclohexane were purchased from Sinopharm Chemical Reagent Co. Ltd (Shanghai, China). Diffuse large B-cell lymphoma cells (DLBCL) were obtained from Fujian Medical University Union Hospital (Fujian, China). Roswell Park Memorial Institute (RPMI-1640) medium, fetal bovine serum (FBS), trypsin (TP), and penicillin-streptomycin (PS) were purchased from Gibco (New York, USA). Phosphate buffer solution (PBS, 1×, 0.0067 M PO_4^{3-}, pH 7.4) was purchased from

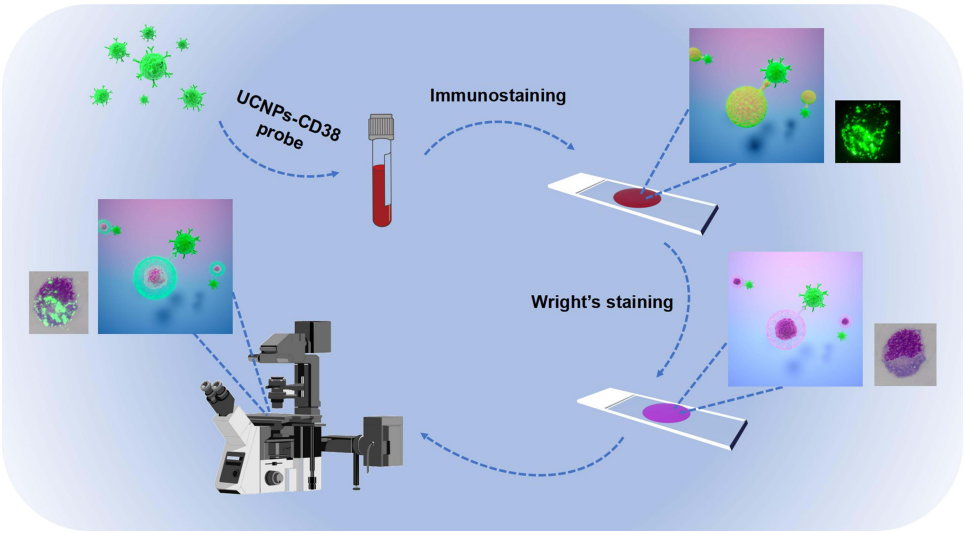

Figure 1 Schematic illustration of a novel leukemia cell identification method based on UCNPs-immunofluorescent staining and Wright's staining.

Hyclone (Utah, USA). Cell counting kit-8 (CCK-8) was purchased from Beyotime (Shanghai, China). Anti-human CD38 monoclonal antibody was obtained from Biolegend (California, US). Adhesive microscope slides were purchased from Citotest (Jiangsu, China).

The characterization of nanomaterial was obtained by a FEI Tecnai F20 transmission electron microscope (TEM, US), a Nicolet iS 10 Fourier transform infrared spectrometer (FTIR, Thermo Fisher Scientific, US), Rigaku SmartLab SE X ray diffractometer (XRD, Japan), and a Litesizer^{TM} 500 particle size and zeta potential analyzer (Anton Paar, Austria). DLBCL cells were characterized by inverted fluorescence microscope (Olympus, Japan) equipped with a 980 nm near-infrared laser with 200× magnification. Cell counting and immunophenotyping were performed with a BD FACSCantoII analytical flow cytometer (Becton, Dickinson and Company, US). The centrifugation method was performed on a LD-ZPJ liquid-based thin layer cell slicing machine (Landing Medical High-tech Co., Ltd, Wuhan, China).

Synthesis and Characterization of $NaYF_4$:Yb,Er UCNPs

According to literature after modification,[24] $NaYF_4$:Yb,Er UCNPs were synthesized by hydrothermal method. Then 0.273 g yttrium acetate tetrahydrate, 0.0084 g erbium acetate hydrate, 0.076 g ytterbium acetate, 0.272 g sodium acetate, 10 mL OA, and 10 mL ODE were mixed in a two-neck flask using a magnetic stirrer. The mixture was heated at 180°C for 20 minutes. After cooling down to room temperature, 0.124 g sodium bifluoride was added. The mixture was heated at 250°C for 30 minutes and further heated at 310°C for 30 minutes. After the hydrothermal reaction, the product ($NaYF_4$:Yb,Er UCNPs) was cooled down naturally, collected by centrifugation (12,000 rpm, 10 minutes), and rinsed three times. The rinsing process was that UCNPs were completely dispersed via ultrasonic treatment in 2 mL cyclohexane for 5 minutes, then precipitated by 4 mL ethanol addition and centrifugation (12,000 rpm, 10 minutes).

For TEM observation, 100 μL of *ca*. 50 μg/mL $NaYF_4$:Yb,Er UCNPs was dropped on the hydrophobic plastic wrap, then the copper mesh was placed over the drop for 5 minutes. After drying naturally, the copper mesh was observed under TEM. For FTIR investigation, the freeze-dried $NaYF_4$:Yb,Er UCNPs were fully mixed with potassium bromide powder, and the mixture was pressed into a flake for detection. For zeta potential measurement, 0.25 mL of *ca*. 50 μg/mL $NaYF_4$:Yb,Er UCNPs was added in a cuvette and measured according to the instructions.

Surface Modification and Probe Construction

The functionalized process was performed according to literature after improvement.[25] The as-prepared $NaYF_4$:Yb,Er UCNPs were firstly transferred into water phase via ultrasonic treatment in acetone for *ca*. 1 hour, centrifugation (12,000 rpm, 10 minutes), and dispersion in ultrapure water. Then, UCNPs were rinsed with ultrapure water three times. The process of rinsing UCNPs with ultrapure water was ultrasonic processing for 5 minutes and centrifugation at 12,000 rpm for 10 minutes. Unless otherwise specified, the following cleaning procedure with ultrapure water was the same as this one. The hydrophilic UCNPs were further treated with 1% PAA solution for 1 hour under shaking conditions to equip with carboxyl groups for downstream antibody conjugation. The prepared UCNPs-PAA was then incubated with 10 mg EDC and 10 mg NHS in 1 mL MES buffer (50 mM, pH 6.0) at room temperature for 30 minutes, centrifuged at 12,000 rpm for 10 minutes and washed with ultrapure water three times. The carboxy groups of PAA-functionalized UCNPs were activated by EDC/NHS coupling reaction for further antibody conjugation via amide bond. After that, the activated UCNPs were respectively incubated with CD38 antibody at different dosages (5, 10, and 20 μg) in hydroxyethyethyl piperazine ethanesulfonic acid buffer solution (HEPES, 50 mM, pH 7.4) for 120 minutes, centrifuged (12,000 rpm, 10 minutes), and washed with ultrapure water three times. Then, CD38-conjugated UCNPs were blocked with 5% BSA for 1 hour under shaking conditions, followed by washing with HEPES (ultrasonic treatment for 5 minutes and centrifugation at 12,000 rpm for 10 minutes) three times to obtain UCNPs-CD38 immunofluorescence probes.

DLBCL Cell Culture, Staining, and Observation

DLBCL cells were cultured in RPMI 1640 medium involving 10% FBS and 1% PS in the humidified atmosphere with 5% CO_2 at 37°C. About 5×10^5 DLBCL cells in 1 mL PBS (pH 7.4) were incubated with 100 μL UCNPs-CD38 immunofluorescence probes for 15, 30, 60, and 120 minutes, respectively. After labeling, DLBCL cells were washed with PBS three times to remove the unconjugated probes. The washing process of cells was that DLBCL cells were dispersed

in 1 mL PBS with a pasteurized pipette, and then centrifuged at 1,000 rpm for 10 minutes. If not used immediately, DLBCL cells were treated with methanol for 30 minutes followed by rinsing with PBS three times. Then, DLBCL cells were diluted with PBS (5×10^4/mL) and centrifuged to adhesive microscope slides (1,000 rpm, 10 minutes) by a liquid-based thin layer cell slicing machine. The prepared slides were treated with Wright's staining for 40 minutes and finally washed with running water for *ca*. 1 minute. After drying in the air, the slides were observed under an inverted fluorescence microscope at 980 nm with excitation power of 1.12 W and an exposure time of 20 seconds. The immunofluorescence intensity was processed with gray intensity analysis of Image J software. The average gray value was obtained by dividing the gray value by the number of cells.

Cytotoxicity Assay

The biocompatibility of UCNPs was measured via CCK-8 assay. DLBCL cells were seeded into 96-well plates within 1.5×10^4 cells per well. The cells were treated with 0, 43.75, 87.5, 175, 350, and 700 μg/mL $NaYF_4$:Yb,Er UCNPs for 24 hours. After incubation, 10 μL CCK-8 solution was added to each well, incubated for 3 hours at 37°C, and measured at 450 nm by microplate spectrophotometer. The cell viability was calculated as the ratio of the absorbance of various groups to the control group.

Real Sample Analysis

Firstly, the blood/bone marrow samples obtained from patients were counted and the concentration of leucocyte was diluted to 1×10^6/mL with PBS. Then, 100 μL cell suspension was placed in a flow cytometer tube and incubated with 20 μL UCNPs-CD38 immunofluorescence probes for 60 minutes at room temperature in the dark. After incubation, the cells were centrifuged (1,000 rpm, 5 minutes) and washed with PBS three times to remove the unconjugated probes. Then, cells were dispersed with PBS (leucocyte $\leq 1\times10^5$/mL) and centrifuged to adhesive microscope slides (1,000 rpm, 10 minutes). The prepared slides were treated with Wright's staining for 40 minutes and finally washed with running water for *ca*. 1 minute. All experiments involving blood samples and bone marrow samples (n=3) were approved by the Ethics Committee of Fujian Medical University Union Hospital (Approval No. 2020WSJK032) and all donors signed their informed consent in accordance with the Declaration of Helsinki.

Statistical Analysis

Student's *t*-test was performed for comparison between different groups for statistical significance using GraphPad Prism 8, and all data were presented as the mean ± SD of at least three independent experiments. The significance level is indicated as **** for $P < 0.0001$, *** for $P < 0.001$, ** for $P < 0.01$, * for $P < 0.05$, or ns for $P > 0.05$.

Results and Discussion

Characterization of $NaYF_4$:Yb,Er UCNPs

$NaYF_4$:Yb,Er UCNPs consisted of a hexagonal (β) $NaYF_4$ host matrix doped with lanthanide ions served as sensitizers (Yb^{3+}) and activator ions (Er^{3+}). The morphology of $NaYF_4$:Yb,Er UCNPs was characterized by TEM. In Figure 2A, $NaYF_4$:Yb,Er UCNPs exhibited a hexagonal crystalline structure. High-resolution TEM (HRTEM) image showed legible lattice fringes with the typical 0.52 nm lattice spacing of (100) crystallographic planes of β-$NaYF_4$ (Figure 2B). In addition, the crystal structure of the prepared UCNPs was identified by XRD. In Figure 2C, the diffraction peaks well matched with hexagonal-phase $NaYF_4$ structure (JCPDS No. 28–1192). FTIR spectrum (Figure 2D) demonstrated that two peaks at 1,560 and 1,460 cm^{-1} were, respectively, attributed to the asymmetric and symmetric stretching vibrations of the carboxylic group (COO^-), and two peaks at 2,930 and 2,860 cm^{-1} were, respectively, associated with the asymmetric and symmetric stretching vibrations of the methylene group, which was consistent with the reported paper.[26] The results confirmed the successful synthesis of $NaYF_4$:Yb,Er UCNPs. To investigate the upconversion photoluminescence properties, the fluorescence spectra at 980 nm with different excitation powers (0.2, 0.5, and 1.12 W) were characterized. As shown in Figure 2E, when the excitation power increased, the intensity of green and red emissions improved. Moreover, three broad emission bands from green to red were observed. Specifically, two green emissions at 522 and 541 nm could be assigned to the $^2H_{11/2}\rightarrow{}^4I_{15/2}$ and ^{4}

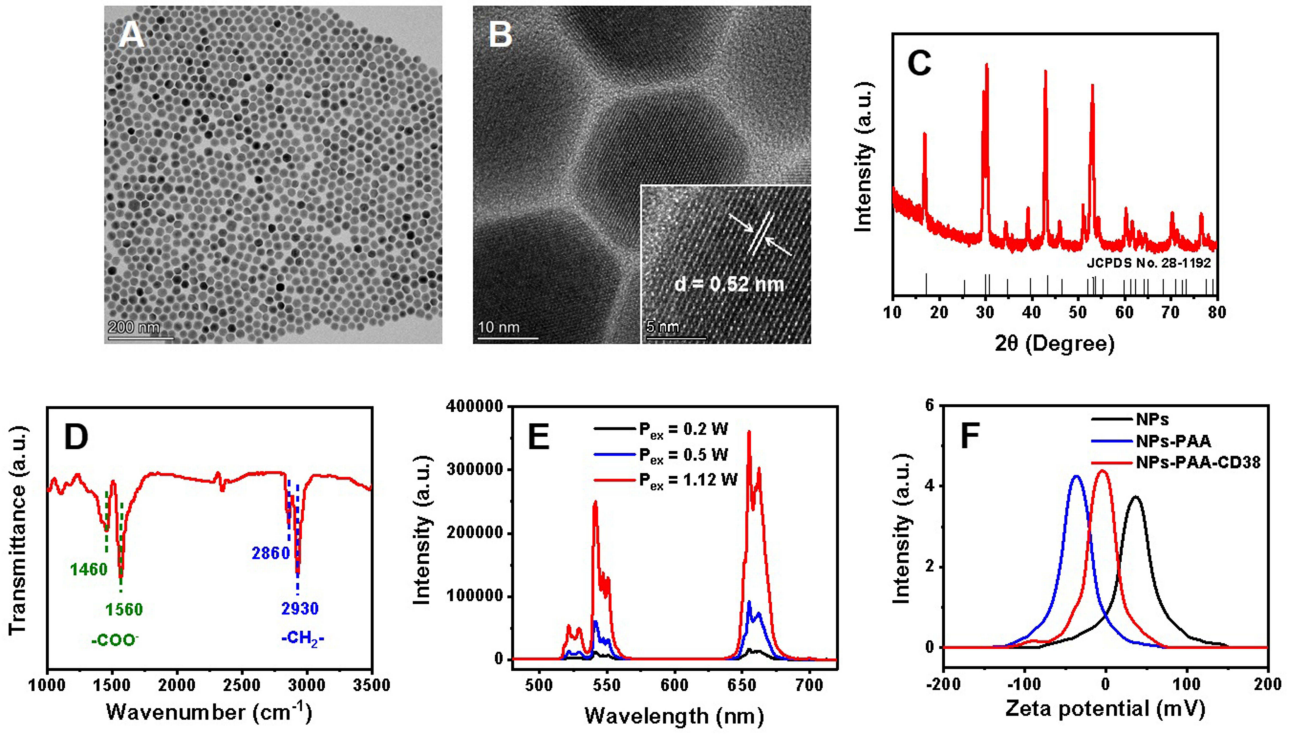

Figure 2 TEM image (**A**), HRTEM image (**B**), XRD spectrum (**C**), and FTIR spectrum (**D**) of $NaYF_4$:Yb,Er UCNPs. (**E**) Upconversion photoluminescence spectra of $NaYF_4$:Yb,Er UCNPs at 980 nm with different excitation powers (0.2, 0.5, and 1.12 W). (**F**) Zeta potential measurements of $NaYF_4$:Yb,Er UCNPs with different surface properties.

$S_{3/2} \rightarrow {}^4I_{15/2}$ transitions, respectively, and the red emission at 655.5 nm was associated with the ${}^4F_{9/2} \rightarrow {}^4I_{15/2}$ transition.[27] Furthermore, we verified the conjugation of $NaYF_4$:Yb,Er UCNPs with CD38 antibody via zeta potential measurements. Figure 2F shows the zeta potentials of UCNPs with various surface properties. The $NaYF_4$:Yb,Er UCNPs after acetone treatment exhibited a positive surface charge of 37.38 mV. After PAA modification, UCNPs-PAA displayed a negative charge around −20.19 mV. After antibody coupling, the UCNPs-PAA-CD38 showed a less negative charge of −9.97 mV. Because the isoelectric point (pI) of CD38 is 8.2, CD38 exhibited a positive surface charge in a neutral PBS environment. The zeta potential change indicated the successful conjugation process.

Biocompatibility of $NaYF_4$:Yb,Er UCNPs

Biocompatibility is a key aspect toward biological application. The cytotoxicity of $NaYF_4$:Yb,Er UCNPs was assessed using a conventional CCK-8 assay. In Figure 3A, the viability of DLBCL cells retained 89.99±3.46% after 24 hours incubation with hydrophilic $NaYF_4$:Yb,Er UCNPs (700 μg/mL). The result illustrated UCNPs possessed good biocompatibility and were suitable for living cell imaging application.

Optimization of Cell Labeling Conditions

Optimization of Medium and Slice-Making Method

To obtain a high performance of cell imaging, the medium and slice-making method were firstly studied. Through acquiring images of different areas randomly, cell number as evaluation index was counted. In Supplementary Figure S1, cells were not evenly dispersed in FBS, but cells were dispersed uniformly in PBS. There were some salt crystals observed in PBS groups, but the crystallization could dissolve via simple washing with a negligible effect on cell adhesion. Considering the cost saving, we adopted the tactic that DLBCL cells dispersed in PBS. Furthermore, slice-making methods (drop-casting method, centrifugation method, and push method) were studied. The result showed the cell number was more uniform and little salt crystals generated

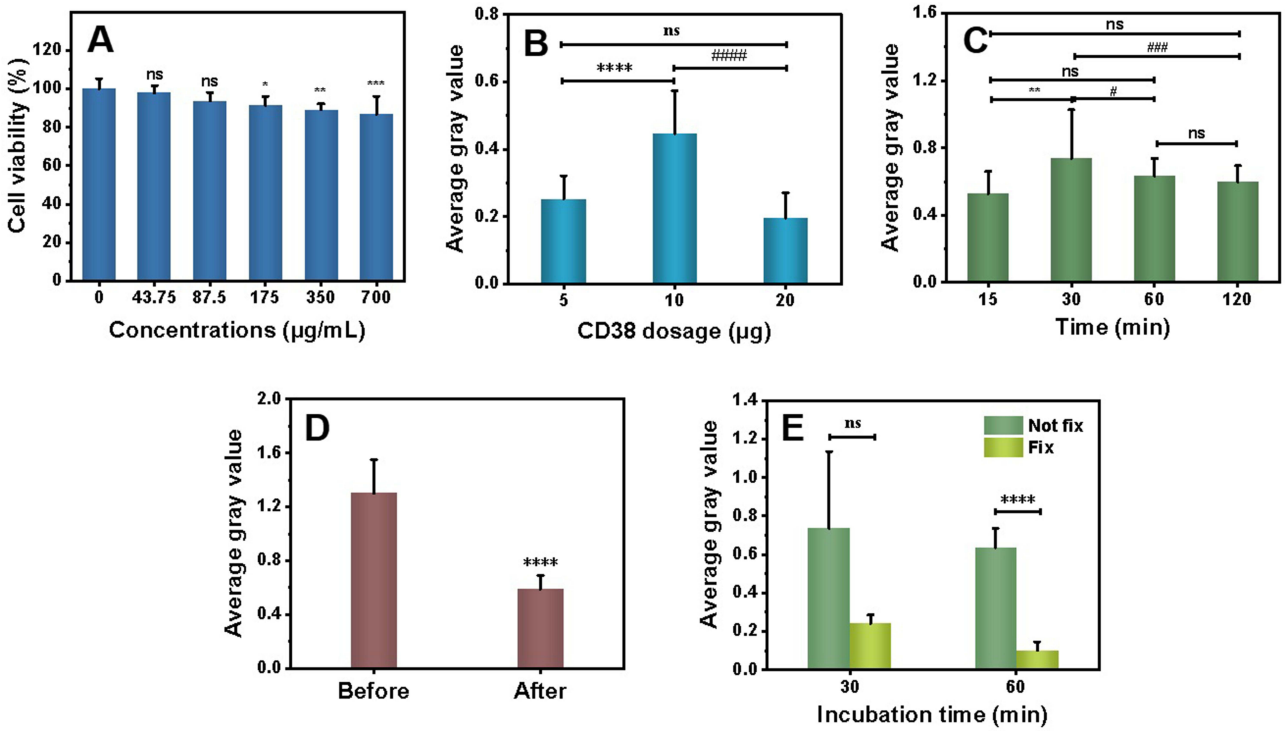

Figure 3 (**A**) CCK-8 assay of DLBCL cells after incubation with $NaYF_4$:Yb,Er UCNPs for 24 hours. Optimization of CD38 dosage (**B**) and incubation time (**C**). Study on the effect of Wright's staining (**D**) and methanol (**E**) on average gray value. Compared between two groups, $^{****}P < 0.0001$, $^{***}P < 0.001$, $^{**}P < 0.01$, $^{*}P < 0.05$, $^{\#\#\#\#}P < 0.0001$, $^{\#\#\#}P < 0.001$, $^{\#}P < 0.05$, ns > 0.05.

via the centrifugation method (Supplementary Figure S1). In view of the homogeneity and repeatability, the centrifugation method was selected as the optimal method.

Optimization of CD38 Dosage

DLBCL cells cultured with different proportions of CD38-conjugated UCNPs (5, 10, and 20 μg CD38 dosage in 1 mL of 700 μg/mL $NaYF_4$:Yb,Er UCNPs solution) were also studied. As shown in Figure 3B, the mean gray values were 0.25 ±0.07, 0.45±0.13, and 0.20±0.08, respectively. As the antibodies increased, immunoreaction became more complete. But when CD38 further increased, the binding efficiency obviously reduced (P<0.0001). Hence, the ratio of 10 μg CD38 to 1 mL of 700 μg/mL UCNPs was selected as optimal dosage.

Optimization of Incubation Time

DLBCL cells incubated with UCNPs-CD38 immunofluorescence probes for different time periods were studied in Figure 3C. When the incubation time was 15 minutes, the gray value per cell was 0.53±0.13. With the time extended to 30 minutes, the average gray value (0.74±0.40) enhanced, indicating the relatively complete immunoreaction. However, the standard deviation value was relatively large, manifesting the cell heterogeneity in immunostaining. After a longer period of incubation, such as 60 and 120 minutes, the mean gray values were 0.64±0.10 and 0.60±0.10, respectively. Importantly, there was no statistical difference (P>0.05) between the average gray values of any two groups. In consideration of time saving and labeling efficiency, 60 minutes was chosen as the optimal incubation time.

Study on Post-Treatment Effect

Further, we investigated the effect of Wright's staining and fixative (methanol) on labeling efficiency. In Figure 3D, before and after Wright's staining, the gray values were 1.30±0.25 and 0.59±0.10, respectively. The difference was statistically significant (P<0.0001). The fluorescence intensity merely maintained 45.29%, because methanol could disrupt antigen-antibody binding,[28,29] manifesting the loss of immunolabeling, and thus Wright's staining needs to be optimized in future studies. We allowed for the case where the sample was not used in time, so the sample needed to be

fixed to maintain cell morphology. In Figure 3E, the average gray values decreased to 0.24±0.04 (ns, P=0.601) and 0.10 ±0.04 (P<0.0001) after 30 and 60 minutes incubation, respectively. The result showed the obvious damage of methanol to cellular fluorescence intensity, so the sample preparation must be achieved in time. To decrease the adverse effect on the overall diagnosis, the samples could be observed using the oil immersion lens of the microscope. As shown in Supplementary Figure S2, the fluorescence intensity was amplified and cell morphology was maintained well under the oil immersion lens of the microscope. Hence, the overall diagnosis will not be influenced.

Analytical Performance Investigation

Considering the relatively homogeneous fluorescence intensity of individual cells, it is reasonable to evaluate the count of DLBCL cells via measuring gray values obtained by Image J software for realizing the rapid diagnosis of leukemia. As shown in Figure 4A, the gray value increased greatly, corresponding to the count of cells from 1 to 32 cells in which the higher the number of cells, the higher the gray value. The regression equation was y=0.49x−0.05 (R^2=0.93) with a limit of detection (LOD) of 1.54 cell/slice (>3 σ/s). In addition, the labeling experiment was repeated three times, three images were randomly taken each time and the gray values per cell were measured. In Figure 4B, the relative standard deviation (RSD) for nine slices was evaluated to be 5.74%, illustrating the excellent reproducibility of UCNPs-CD38 immunofluorescence probe. Subsequently, the stability of the samples (UCNPs-CD38 immunofluorescence probe labeled DLBCL cells) was studied. The average gray value maintained 91.20% of its original value after 5 days (Figure 4C, ns, P=0.59), demonstrating the good storage stability. Taken together, the UCNPs-CD38 immunofluorescence probe was capable of realizing qualitative and quantitative detection of target cells, and further achieving rapid diagnosis of leukemia.

Cell Imaging Study

To investigate the commonality of synchronous detection method, we chose CD38 as a proof of concept due to its high expression in DLBCL. Four groups of DLBCL cells are observed in Figure 5, that is, the fixed DLBCL cells (blank control group), cells only treated with Wright's staining, cells merely labeled with UCNPs-CD38 immunofluorescence probe, and cells labeled with UCNPs-CD38 immunofluorescence probe accompanied by Wright's staining. In the blank control group (Figure 5A), DLBCL cells did not emit any fluorescence under a 980 nm laser, demonstrating the infrared light is able to effectively avoid autofluorescence from biological samples. Figure 5B displays the typical cytoplasm and nucleus structures after Wright's staining. In Figure 5C, intense green luminescent emission from $NaYF_4$:Yb,Er UCNPs can be observed in DLBCL cells. The merged image exhibited clearly that the immunoprobes coupled to the cell surface. After Wright's staining, the cellular fluorescence intensity reduced to a certain extent (Figure 5D), which was consistent with the aforementioned result (Figure 4D). The overlay of bright field image and fluorescence image illustrated the feasibility of rapidly and specifically morphological and immunologic diagnoses of leukemia.

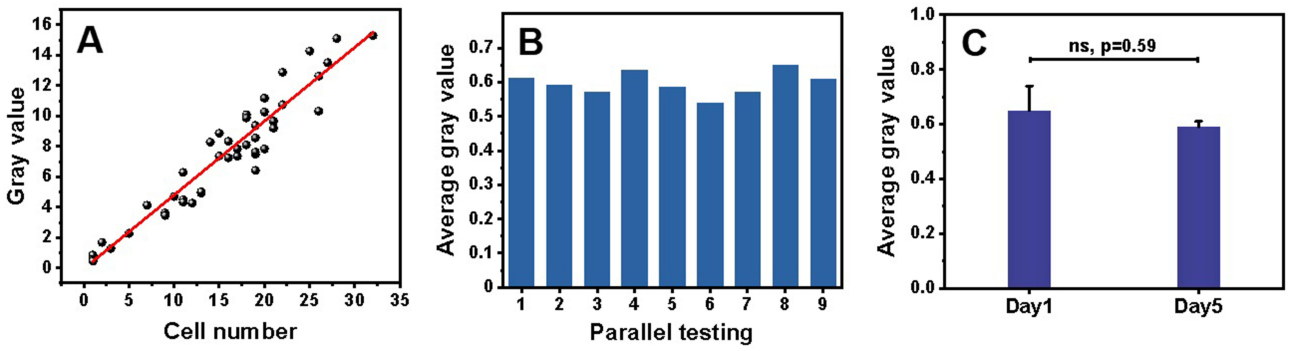

Figure 4 (**A**) Linear relationship between gray value and number of DLBCL cells. Reproducibility (**B**) and stability (**C**) of UCNPs-CD38 immunofluorescence probes labeled with DLBCL cells. Compared between two groups, ns > 0.05.

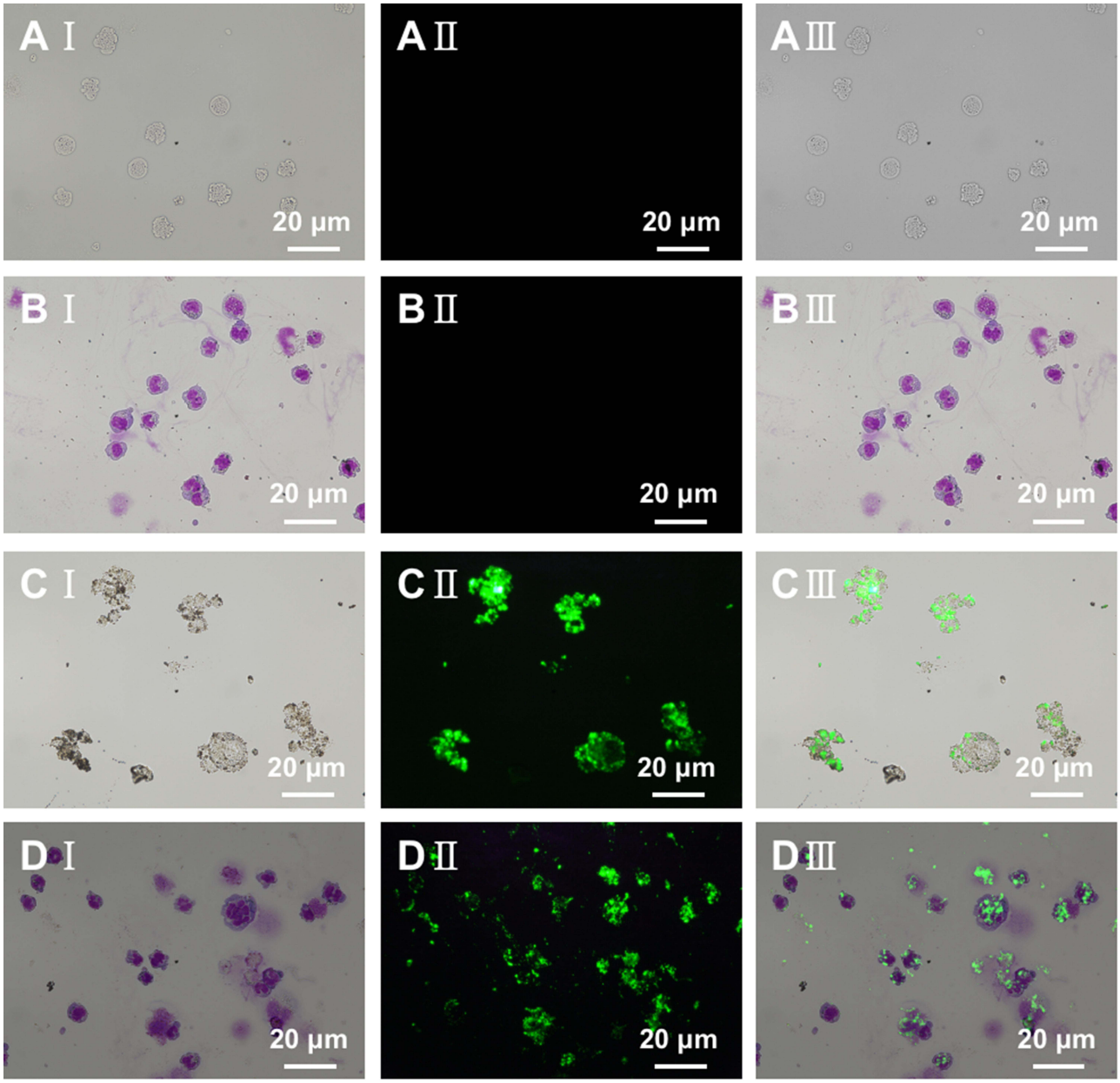

Figure 5 Bright-field optical images, fluorescence images, and merged images of DLBCL cells with various treatment. (**A**) DLBCL cells treated with methanol (blank control group). (**B**) DLBCL cells only treated with Wright's staining. (**C**) DLBCL cells merely labeled with UCNPs-CD38 immunofluorescence probes. (**D**) DLBCL cells labeled with UCNPs-CD38 immunofluorescence probes accompanied by Wright's staining.

Real Sample Analysis

Morphological diagnosis of blood and bone marrow smear, providing the features and differential counts of the blasts, remains a basic tool. Immunophenotypic characterization, as a powerful auxiliary tool, delineates cell surface and cytoplasmic biomarkers. Morphological method supplemented with immunophenotyping drives the decision-making for diagnosis and a specific therapeutic regimen. In this part, according to the aforementioned experimental process, we collected and assessed blood samples or bone marrow samples of three cases (the patients diagnosed with leukemia) from Fujian Medical University Union Hospital. As shown in Figure 6 and Supplementary Table S1, the samples were obtained from the patients diagnosed with subtype M_{5b} acute myelocytic leukemia (AML, blood sample), small B-cell lymphoma/leukemia (non CLL, bone marrow sample), and subtype M_{5b} AML (blood sample). Among them, only the third blood sample was treated with whole blood red cell lysing reagent for 10 minutes. The results exhibited that, after Wright's staining, the leucocytes and red blood cells were all well colored (Figure 6AI, BI, and CI). In Figure 6AII, after

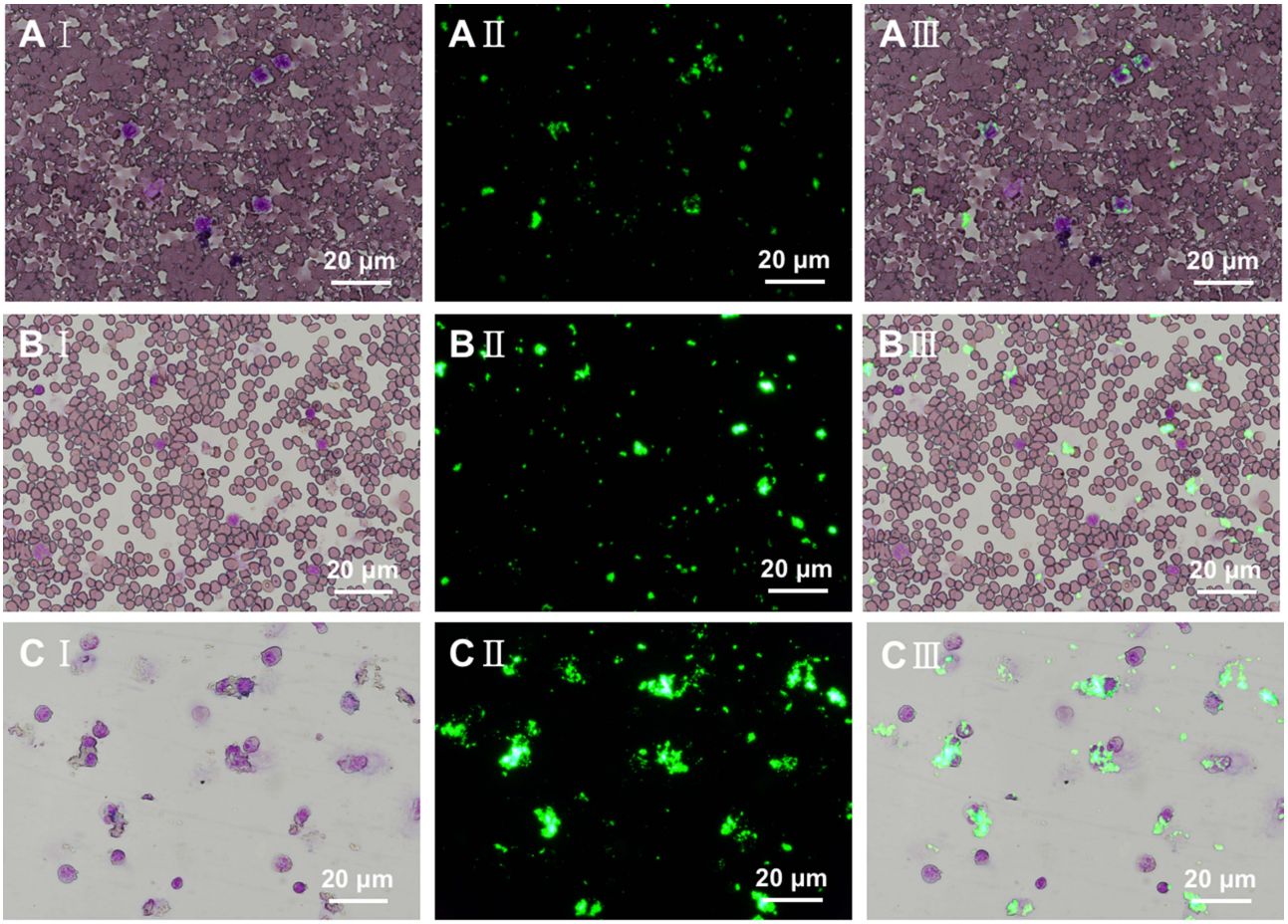

Figure 6 Bright-field optical image, fluorescence image and merged image of peripheral blood or bone marrow samples from patients diagnosed with subtype M_{5b} AML (**A**), small B-cell lymphoma/leukemia (non CLL) (**B**), and subtype M_{5b} AML (**C**).

incubation with UCNPs-CD38 immunoflurescence probes, the leucocytes were obviously stained, but some red blood cells also exhibited slight green fluorescence. Fortunately, the overlapped image (Figure 6AIII) showed the unique morphological features and distinctly green luminescence of leucocytes which could be easily distinguished with red blood cells, demonstrating the immunostaining CD38-positive result. On the basis of preliminary diagnosis (subtype M_{5b} AML) and FCM result (CD38-positive rate: 13.40%), the imaging result of the first patient was consistent. In Figure 6BII, the patient was diagnosed with small B-cell lymphoma/leukemia (non CLL), so theoretically the CD38 antigen was negative. However, there were still some probes that remained irregularly on the adhesive microscope slide, which was prone to a false positive result via a single immunolabeling mode. Supplemented with cytomorphological characteristics under a bright field microscope, the overlapped image displayed that the green luminescence and cells were not co-localized, indicating the immunostaining result was negative (Figure 6BIII), which agreed with the CD38-negative FCM result. Furthermore, considering the interference of non-specific binding between red cells and probes, the third blood sample was pre-treated with whole blood red cell lysing reagent. As displayed in Figure 6CI–CIII, the leucocytes could be observed clearly, and the cells manifested brightly green fluorescence, which was also in accordance with clinical diagnosis (subtype M_{5b} AML) and FCM result (CD38-positive rate: 88.20%). The above results indicate the proposed tactic could realize simultaneous determination of cytomorphology and immunophenotyping, possessing great potential in accurate, rapid, and low-cost leukemia diagnosis.

Conclusions

In sum, a synergetic recognition method based on Wright's staining (cytomorphology) and $NaYF_4$:Yb,Er UCNPs-CD38 immunofluorescence probe labeling (immunophenotyping) was prepared for leukemia cell imaging and clinical diagnosis. In this approach, both cell morphology and immunolabeling could be visually determined. Compared with other methods for diagnoses of leukemia, as shown in Supplementary Table S2, this integrative approach possessed merits of simple operation, rapidness, low cost, and high sensitivity, which providing an alternative for conventional bone marrow smear assay for early diagnosis of leukemia. However, this experiment still has some shortcomings, and further work is underway to design the multi-combination of UCNPs-antibodies for diagnosis verification, extend the storage time of samples, and reduce the effect of Wright's staining or methanol fixation on immunolabeling intensity.

Acknowledgments

The authors gratefully acknowledge the Fujian Provincial University-Industry Cooperation Science & Technology Major Program (2019Y4006), Construction project of Fujian Medical Center of Hematology (Min201704), National and Fujian Provincial Key Clinical Specialty Discipline Construction Program, P. R.C for financial support.

Disclosure

Dr Fei Gao reports a pending patent "Accurate diagnosis of leukemia cells based on rare earth nanomaterial immunolabeling technology combined with cell morphology technology". The authors declare that they have no other known competing financial interests or personal relationships that could have appeared to influence the work reported in this paper.

References

1. Whiteley AE, Price TT, Cantelli G, Sipkins DA. Leukaemia: a model metastatic disease. *Nat Rev Cancer*. 2021;21(7):461–475. doi:10.1038/s41568-021-00355-z
2. Cobaleda C, Vicente-Dueñas C, Sanchez-Garcia I. Infectious triggers and novel therapeutic opportunities in childhood B cell leukaemia. *Nat Rev Immunol*. 2021;21(9):570–581. doi:10.1038/s41577-021-00505-2
3. Haferlach T, Schmidts I. The power and potential of integrated diagnostics in acute myeloid leukaemia. *Brit J Haematol*. 2020;188(1):36–48. doi:10.1111/bjh.16360
4. Malard F, Mohty M. Acute lymphoblastic leukaemia. *Lancet*. 2020;395(10230):1146–1162. doi:10.1016/S0140-6736(19)33018-1
5. Harrington P, de Lavallade H. Novel developments in chronic myeloid leukaemia. *Curr Opin Hematol*. 2021;28(2):122–127. doi:10.1097/MOH.0000000000000630
6. Hur M, Cho JH, Kim H, et al. Optimization of laboratory workflow in clinical hematology laboratory with reduced manual slide review: comparison between Sysmex XE-2100 and ABX Pentra DX120. *Int J Lab Hematol*. 2011;33(4):434–440. doi:10.1111/j.1751-553X.2011.01306.x
7. Haferlach T, Kern W, Schnittger S, Schoch C. Modern diagnostics in acute leukemias. *Crit Rev Oncol Hemat*. 2005;56(2):223–234. doi:10.1016/j.critrevonc.2004.04.008
8. Frater JL, Shirai CL, Brestoff JR. Technological features of blast identification in the cerebrospinal fluid: a systematic review of flow cytometry and laboratory haematology methods. *Int J Lab Hematol*. 2022;44:45–53. doi:10.1111/ijlh.13869
9. Loghavi S, DiNardo CD, Furudate K, et al. Flow cytometric immunophenotypic alterations of persistent clonal haematopoiesis in remission bone marrows of patients with NPM1-mutated acute myeloid leukaemia. *Brit J Haematol*. 2021;192(6):1054–1063. doi:10.1111/bjh.17347
10. Camburn AE, Petrasich M, Ruskova A, Chan G. Myeloblasts in normal bone marrows expressing leukaemia-associated immunophenotypes. *Pathology*. 2019;51(5):502–506. doi:10.1016/j.pathol.2019.03.010
11. Rawstron AC, Villamor N, Ritgen M, et al. International standardized approach for flow cytometric residual disease monitoring in chronic lymphocytic leukaemia. *Leukemia*. 2007;21(5):956–964. doi:10.1038/sj.leu.2404584
12. Ernst P, Press AT, Fischer M, et al. Polymethine dye-functionalized nanoparticles for targeting CML stem cells. *Mol Ther Oncolytics*. 2020;18:372–381. doi:10.1016/j.omto.2020.07.007
13. Wu X, Liu H, Liu J, et al. Immunofluorescent labeling of cancer marker Her2 and other cellular targets with semiconductor quantum dots. *Nat Biotechnol*. 2003;21(1):41–46. doi:10.1038/nbt764
14. Xi Y, Wang D, Wang T, Huang L, Zhang XE. Quantitative profiling of CD13 on single acute myeloid leukemia cells by super-resolution imaging and its implication in targeted drug susceptibility assessment. *Nanoscale*. 2019;11(4):1737–1744. doi:10.1039/C8NR06526H
15. Best TP, Edelson BS, Nickols NG, Dervan PB. Nuclear localization of pyrrole-imidazole polyamide-fluorescein conjugates in cell culture. *P Natl Acad Sci USA*. 2003;100(21):12063–12068. doi:10.1073/pnas.2035074100
16. Wen S, Zhou J, Zheng K, Bednarkiewicz A, Liu X, Jin D. Advances in highly doped upconversion nanoparticles. *Nat Commun*. 2018;9(1):1–12. doi:10.1038/s41467-018-04813-5
17. Zhang Y, Zhu X, Zhang Y. Exploring heterostructured upconversion nanoparticles: from rational engineering to diverse applications. *ACS Nano*. 2021;15(3):3709–3735. doi:10.1021/acsnano.0c09231
18. Zhu X, Zhang J, Liu J, Zhang Y. Recent progress of rare-earth doped upconversion nanoparticles: synthesis, optimization, and applications. *Adv Sci*. 2019;6(22):1901358. doi:10.1002/advs.201901358

19. Liu C, Zheng X, Dai T, et al. Reversibly photoswitching upconversion nanoparticles for super-sensitive photoacoustic molecular imaging. *Angew Chem Int Edit*. 2022;134(19):e202116802. doi:10.1002/ange.202116802
20. Dubey N, Chandra S. Upconversion nanoparticles: recent strategies and mechanism based applications. *J Rare Earth*. 2022;40(9):1343–1359. doi:10.1016/j.jre.2022.04.015
21. Hlaváček A, Farka Z, Mickert MJ, et al. Bioconjugates of photon-upconversion nanoparticles for cancer biomarker detection and imaging. *Nat Protoc*. 2022;17(4):1028–1072. doi:10.1038/s41596-021-00670-7
22. Thu Huong T, Thi Phuong H, Thi Vinh L, et al. Upconversion $NaYF_4$:Yb^{3+}/Er^{3+}@silica-TPGS bio-nano complexes: synthesis, characterization, and in vitro tests for labeling cancer cells. *J Phys Chem B*. 2021;125(34):9768–9775. doi:10.1021/acs.jpcb.1c05472
23. Wada F, Shimomura Y, Yabushita T, et al. CD38 expression is an important prognostic marker in diffuse large B-cell lymphoma. *Hematol Oncol*. 2021;39(4):483–489. doi:10.1002/hon.2904
24. Li H, Shi X, Li X, Zong L. Size-tunable β-$NaYF_4$:Yb/Er up-converting nanoparticles with a strong green emission synthesized by thermal decomposition. *Opt Mater*. 2020;108:110144. doi:10.1016/j.optmat.2020.110144
25. Guo H, Song X, Lei W, et al. Direct detection of circulating tumor cells in whole blood using time-resolved luminescent lanthanide nanoprobes. *Angew Chem Int Edit*. 2019;58(35):12195–12199. doi:10.1002/anie.201907605
26. Wang M, Mi CC, Wang WX, et al. Immunolabeling and NIR-excited fluorescent imaging of HeLa cells by using $NaYF_4$:Yb,Er upconversion nanoparticles. *ACS Nano*. 2009;3(6):1580–1586. doi:10.1021/nn900491j
27. Mi C, Tian Z, Cao C, Wang Z, Mao C, Xu S. Novel microwave-assisted solvothermal synthesis of $NaYF_4$:Yb,Er upconversion nanoparticles and their application in cancer cell imaging. *Langmuir*. 2011;27(23):14632–14637. doi:10.1021/la204015m
28. Haas GG, DeBault LE, D'Cruz O, Shuey R. The effect of fixatives and/or air-drying on the plasma and acrosomal membranes of human sperm. *Fertil Steril*. 1988;50(3):487–492. doi:10.1016/S0015-0282(16)60138-3
29. Prince AE, Fan TS, Skoczenski BA, Bushway RJ. Development of an immunoaffinity-based solid-phase extraction for diazinon. *Anal Chim Acta*. 2001;444(1):37–49. doi:10.1016/S0003-2670(01)01149-7